State-specific dissociation enhancement of ionic and excited neutral photofragments of gaseous CCl_4 and solid-state analogs following Cl 2p core-level excitation

2008 New J. Phys. 10 053009

(http://iopscience.iop.org/1367-2630/10/5/053009)

New Journal of Physics
The open-access journal for physics

State-specific dissociation enhancement of ionic and excited neutral photofragments of gaseous CCl_4 and solid-state analogs following Cl 2p core-level excitation

K T Lu[1,3], J M Chen[1,3], J M Lee[1,2], C K Chen[1], T L Chou[1] and H C Chen[1]

[1] National Synchrotron Radiation Research Center (NSRRC), Hsinchu, 30076 Taiwan, Republic of China
[2] Department of Electrophysics, National Chiao Tung University, Hsinchu, 30010 Taiwan, Republic of China
E-mail: ktlu@nsrrc.org.tw and jmchen@nsrrc.org.tw

New Journal of Physics **10** (2008) 053009 (13pp)
Received 28 February 2008
Published 7 May 2008
Online at http://www.njp.org/
doi:10.1088/1367-2630/10/5/053009

Abstract. The state-selective dissociation pathways for ionic and excited neutral fragments of gaseous and condensed CCl_4 following Cl 2p core-level excitation have been characterized by combining photon-induced ionic dissociation, x-ray absorption, resonant photoemission and UV/visible dispersed fluorescence measurements. The Cl $2p \rightarrow 7a_1^*$ excitation of CCl_4 induces significant enhancement of the Cl^+ desorption yield in the condensed phase and the CCl^+ yields in the gaseous phase. Based on the resonant photoemission studies, excitations of Cl 2p electrons to valence orbitals and Rydberg states decay predominantly via the spectator Auger transitions. The transitions of Cl 2p electrons to the Rydberg state of gaseous CCl_4 lead to a noteworthy production of excited atomic neutral fragments (C^*) and excited diatomic neutral fragments (CCl^*). These results provide insight into the state-selective ionic and neutral fragmentation processes of molecules via core-level excitation.

[3] Authors to whom any correspondence should be addressed.

Contents

1. Introduction

The electronic decay pathways and subsequent profound dissociation dynamics of polyatomic gaseous molecules and molecular adsorbates on surfaces via excitations of x-ray photons have been subjects of extensive research because of their scientific importance and technological applications [1]–[3]. By means of synchrotron radiation with energy tunable in the x-ray region, the site-selective photoexcitation and accordingly preferential cleavage of a specific chemical bond of molecules via core-level excitation have been observed for several systems [4]–[10], but not for some molecules [11, 12]. The intricate fragmentation dynamics of core-excited states of gaseous molecules and solid-state analogs remains a topic of broad interest [13]–[16]. However, the fragmented ions reported in the literature were predominantly positive ions [4]–[8], [13]–[16]. The investigation of the dissociation dynamics of neutral fragments of molecules via inner-shell photoexcitation is still in its infancy [9], [17]–[19]. The investigation of neutral species of gas-phase molecules and molecular adsorbates on surfaces following core-level excitation is a promising field due to the complexity of the new physical processes involved in molecular dissociation. For the gas phase, neutral-fragment measurements are currently very difficult because of the low efficiency of detectors for neutrals. UV/visible dispersed fluorescence measurement in the visible and ultraviolet regions is a powerful method to detect excited neutral and ionic products produced by electronic excitation. Fluorescence excitation spectra provide abundant information about the dissociation dynamics and electronic relaxation processes of core-excited molecules [9]. Besides, the dissociation pathways of core-excited molecules in the solid phase is known to be strongly modified as compared with the gaseous-phase due to an electronic interaction with a substrate and/or neighboring molecules at the solid surface [9]. Accordingly, to elucidate the dissociation dynamics of core-excited molecules, coordinated studies of gaseous-phase molecules and solid-state analogs using various techniques are indispensable. To date, however, there have been relatively few reports of coordinated studies of ionic fragments and neutral fragments produced by inner-shell excitation of molecules.

Carbon tetrachloride (CCl_4) and the freon molecules (CF_nCl_{4-n}, $n = 1$–3) are important atmospheric pollutants, leading to the destruction of ozone [20]. Adsorbed on single-crystalline surfaces, halomethanes are model systems for studies of surface photochemistry [21]. Besides, CCl_4 molecules are also used in reactive ion etching of semiconductors. In this study, we used CCl_4 as a model molecule for investigations of the dissociation dynamics of ionic and neutral fragments of gaseous and condensed CCl_4 following excitations of Cl 2p electrons to various resonances by combining photon-induced ionic dissociation, resonant photoemission, ion kinetic energy distribution, x-ray absorption, and UV/visible dispersed fluorescence

measurements. The most striking observation is that the Cl 2p core-to-Rydberg excitations of gaseous CCl_4 lead to a noteworthy production of excited atomic neutral fragments (C^*) and excited diatomic neutral fragments (CCl^*).

2. Experiments

The experimental measurements were carried out at the high-energy spherical grating monochromator (HSGM) beamline and the U5 undulator beamline coupled with a spherical grating monochromator of the National Synchrotron Radiation Research Center (NSRRC) in Taiwan. For photon stimulated ion desorption (PSID) measurements in the condensed phase, an ultrahigh-vacuum (UHV) chamber with a base pressure of $\sim 1 \times 10^{-10}$ Torr was used. The Si(100) surface was cleaned by repeated resistive heating to $\sim$1100 °C under vacuum before the measurements. High purity CCl_4 (Merck, 99.9%) was degassed by several freeze–pump–thaw cycles before use. The vapor of CCl_4 was then condensed through a leak valve onto the Si(100) surface at $\sim$90 K. The ion desorption yields were detected with a quadrupole mass spectrometer (Balzers model QMA 410 with off-axis secondary electron multiplier). The ion kinetic energy distribution (not calibrated) was measured by a quadrupole mass spectrometer with a 45° sector field analyzer (Hiden, EQS). The quadrupole detector was oriented perpendicular to the substrate surface, and photons were incident at an angle of 45° with respect to the substrate normal. Solid-phase x-ray absorption spectra were recorded in the total-electron yield (TEY) mode using a microchannel plate detector. Photoemission spectra were measured with a double-pass cylindrical mirror analyzer, employing a constant pass energy of 25 eV with energy resolution of the observed electrons $\sim$0.5 eV. The surface coverage was determined by thermal desorption spectroscopy (TDS). The TDS spectra from CCl_4/Si(100) show a single molecular desorption peak of $\sim$139 K with an exposure of 4 L or less. Above 4 L exposure, an additional peak starts appearing at a lower temperature of $\sim$132 K and its intensity increases with exposures. Thus, 4 L exposure of CCl_4 on Si(100) corresponds to one monolayer (ML).

To measure ionic photofragments in the gaseous phase, an effusive molecular beam produced by expanding the gas through an orifice (50 μm) into the experimental chamber was used. The pressure in this chamber was maintained at $\sim 1 \times 10^{-5}$ Torr. Fragment ions were mass-selected with a quadrupole mass spectrometer (Hiden, IDP). UV/visible fluorescence was dispersed by a 0.39 m spectrometer using a $f/1.5$ fused silica extraction optic located normal to and in the plane of polarization of the synchrotron radiation. The fluorescence was then detected by a Hamamatsu R928 photomultiplier tube (PMT). The relative fluorescence signal was not corrected for the efficiency of the PMT. For dispersed fluorescence measurements, the pressure in the effusive beam chamber was kept at $\sim 9 \times 10^{-5}$ Torr. For gaseous-phase photoemission experiments, a supersonic molecular beam is generated by bubbling He gas through CCl_4 in a reservoir and directing it through a continuous-beam nozzle with a seed ratio (concentration ratio of sample gas to He carrier gas) $\sim$10%. Photoemission spectra were measured by a hemispherical electron energy analyzer (VG, Clam4). Gas-phase absorption spectra were measured using an ion chamber with a pressure $\sim 1 \times 10^{-4}$ Torr.

For photodissociation measurements, the HSGM beamline was operated with 100 μm slits corresponding to the energy resolution $\sim$0.2 eV at the Cl 2p edge. To obtain the high-resolution x-ray absorption spectrum, the HSGM beamline was set to a photon resolution $\sim$0.1 eV at the Cl 2p edge. Due to the low signal levels for dispersed fluorescence measurements, the U5 undulator beamline was operated with a 100 μm entrance slit and a 300 μm exit slit

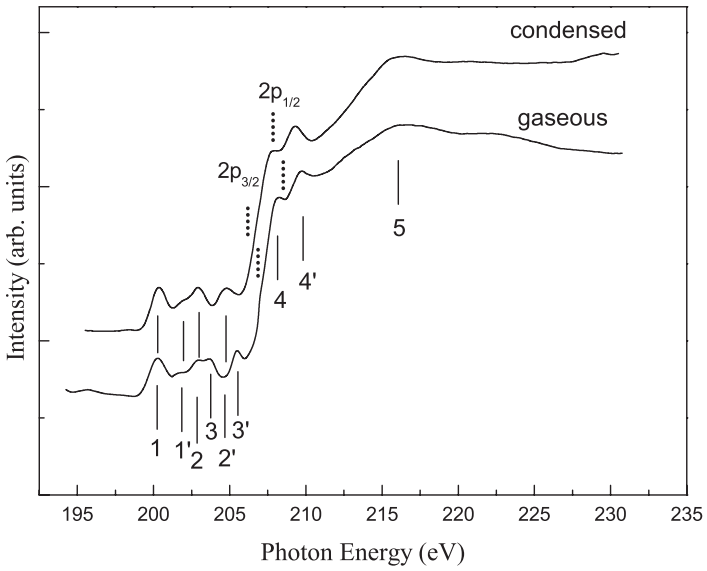

Figure 1. Solid TEY and gas-phase photoabsorption spectra of CCl_4 in the Cl 2p region. As determined by the x-ray photoemission spectra, the $Cl(2p_{3/2})$and $Cl(2p_{1/2})$ ionization thresholds of condensed (206.2 and 207.8 eV) and gaseous (206.9 and 208.5 eV) CCl_4 (from [23]) are indicated. The binding energies are in reference to the vacuum level.

(resolution $=\sim$0.3 at 200 eV), while the spectral resolution of the spectrometer was set to $\sim$10 nm. The incident photon intensity (I_0) was monitored simultaneously by a Ni mesh located after the exit slit of the monochromator. All yield spectra of fragment ions, x-ray absorption spectra, and fluorescence excitation spectra were normalized to the incident photon flux at the Cl 2p edge. The photon energies were calibrated within an accuracy of 0.1 eV using the Si 2p absorption edge (99.76 and 100.37 eV) of Si(100) and Si 2p absorption peaks at 104.1 eV and 104.2 eV in gaseous and solid-phase $SiCl_4$ together with Cl 2p absorption peaks contributed from second-order light of synchrotron radiation at the Si 2p region [22].

3. Results and discussion

The Cl L_{23}-edge x-ray-absorption near-edge structure spectra of condensed and gaseous CCl_4 are displayed in figure 1. The absorption peaks labeled 1 and 1′ are assigned to the transition $Cl\,2p_{1/2,3/2} \rightarrow 7a_1^*$. The features labeled 2 and 2′ correspond to the $Cl\,2p_{1/2,3/2} \rightarrow 8t_2^*$ excitations. It is noted that the absorption features located at 203.9 and 205.5 eV labeled 3 and 3′ in the gas-phase absorption spectrum are smeared out in the solid-phase TEY spectrum. This indicates that these final states (peaks 3 and 3′) should have predominantly Rydberg character. However, in contrast to our assignment, due to poor resolution in the Cl L-edge absorption spectrum of gaseous CCl_4 reported by Hitchcock and Brion [23], only one peak at 203.5 eV was observed and assigned to the transitions into $8t_2^*$ and Rydberg states. Hitchcock and Brion [23], assigned absorption peaks labeled 4 and 4′ to the delay onset of Rydberg transitions or shake-up transitions involving simultaneous excitation of a Cl 2p electron and a valence electron to unoccupied orbitals [23]. As compared with the gas-phase absorption spectrum, absorption

Table 1. Energy positions and the assignments of absorption peaks in the Cl L-edge absorption spectra of gaseous and molecular-solid CCl_4. The energies are expressed in electron volt.

Peak	Peak position		Assignment
	Gaseous	Molecular-solid	
1	200.3	200.4	$7a_1^*$
1′	201.9	202	$7a_1^*$
2	202.9	203	$8t_2^*$
3	203.9		Rydberg state
2′	204.6	204.7	$8t_2^*$
3′	205.5		Rydberg state
4	208.3	207.8	Delay onset and shake-up
4	209.9	209.4	Delay onset and shake-up
5	216	216	Shape resonance

peaks 4 and 4′ are observed with almost equal strength in the solid-phase TEY spectrum, indicating that these peaks have predominantly valence character. Besides, based on present fluorescence excitation spectra (as discussed below), peaks 4 and 4′ have some characters of Rydberg states. It is therefore suggested that discrete peaks 4 and 4′ might be due to the superposition of the Rydberg transitions and shake-up transitions, as proposed by Hitchcock and Brion [23]. The broad peak at ∼216 eV labeled 5 is attributed to a shape resonance. In table 1, we list the energy positions and the assignments of absorption peaks in the Cl L-edge absorption spectra of gaseous and molecular-solid CCl_4. As noted, for absorption peaks with dominant valence and Rydberg characters, upon going from the gas phase to solid phase, there is an energy shift toward higher photon energy of ∼0.1 eV.

In figure 2(a), the PSID spectra of Cl^+, CCl^+, CCl_2^+ and CCl_3^+, along with the Cl L-edge x-ray absorption spectrum recorded by TEY mode, for condensed CCl_4 with multilayer coverage (>100 L exposure) following the Cl 2p core-level excitation are shown. As noted from figure 2(a), the PSID spectra of CCl^+, CCl_2^+ and CCl_3^+ nearly follow the TEY curve of solid CCl_4. In contrast, the Cl^+ PSID spectrum and the Cl L_{23}-edge TEY spectrum of condensed CCl_4 show a significant dissimilarity. The Cl 2p → $7a_1^*$ resonant excitation leads to a significant enhancement of the Cl^+ yield, compared with the transitions Cl 2p → $8t_2^*$ and Cl 2p → Rydberg states. The Cl $2p_{3/2}$ → $7a_1^*$ excitation (absorption peak labeled 1) in condensed CCl_4 gives rise to ∼5 times enhancement of Cl^+ yield, as compared with the intensity ratio of the corresponding transition to the shape resonance at ∼216 eV in the Cl L_{23}-edge TEY spectrum.

In figure 2(b), the fragment ion yields of Cl^+, Cl^{++}, C^+, CCl^+, CCl_2^+ and CCl_3^+ for gaseous CCl_4 following the Cl 2p core-level excitation are reproduced along with the Cl L-edge x-ray absorption spectrum for comparison. As noted from figure 2(b), the photon-energy dependence of yields of various fragment ions, except C^+ and CCl^+, of gaseous CCl_4 exhibits a close resemblance to the Cl L_{23}-edge x-ray absorption spectrum. Especially noteworthy is that the Cl 2p → $7a_1^*$ excitation of gaseous CCl_4 induces an enhanced production of CCl^+ yields. Comparison of the C^+ yield spectrum and the Cl L_{23}-edge absorption spectrum in figure 2(b) shows that the transitions of Cl 2p electrons to Rydberg orbitals (peaks 3 and 3′) and to peaks 4 and 4′ produce an enhancement of the C^+ yield, as compared with the

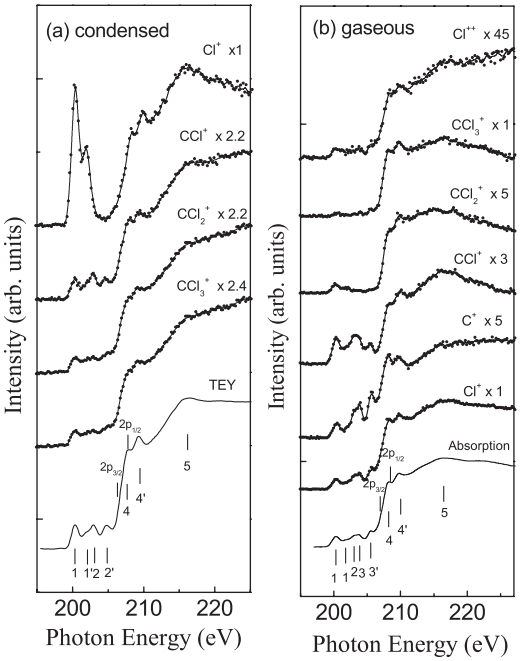

Figure 2. (a) PSID spectra of condensed CCl_4 (>100 L exposure corresponding to ∼25 ML) via the Cl 2p core-level excitation along with the Cl L-edge TEY spectrum. (b) Photon-energy dependence of various fragmented ion yields of gaseous CCl_4 at the Cl 2p edge together with Cl L-edge photoabsorption spectrum. The $Cl(2p_{1/2})$ and $Cl(2p_{3/2})$ ionization thresholds of condensed and gaseous CCl_4 are indicated in the absorption spectrum.

transitions $Cl\,2p \rightarrow 7a_1^*$ and $Cl\,2p \rightarrow 8t_2^*$. As clearly shown in figure 2, there are significant differences in the efficiency for producing fragment ions, even when these transitions arise from the same atomic site. Hence, the orbital character of an excited electron plays a crucial role in determining the photodissociation processes. As noted, CCl_3^+ shows the largest intensity in gaseous CCl_4 following the Cl 2p core-level excitation. In contrast, because CCl_3^+ is heavier, the speed of departure of CCl_3^+ from the surface is smaller. The slow movement of CCl_3^+ and rapid neutralization processes greatly reduce the ion yield in the condensed CCl_4 via the Cl 2p core-level excitation.

To understand the detailed desorption mechanism, we monitored the Auger decay processes following resonant excitations of Cl 2p electrons to various unoccupied orbitals in condensed and gaseous CCl_4. For low-Z elements, the primary de-excitation process following core excitation is an Auger-type transition rather than x-ray fluorescence emission. We therefore focus on the Auger decay processes of core-excited states. In general, the resonant core-excited states with an excited electron in the unoccupied states decay primarily by spectator Auger transition and participant Auger transition [24]. The spectator Auger decay results in a two-hole one-electron (2h1e) final state in which two holes are produced in valence orbitals and one electron is excited into an antibonding valence orbital or a Rydberg orbital. Because the participant Auger decay creates the same final states with one hole (1 h) in the valence band as normal photoemission processes of the valence orbitals, the participant Auger decay manifests itself through enhanced intensity of the corresponding valence-band photoelectron peak. Thus,

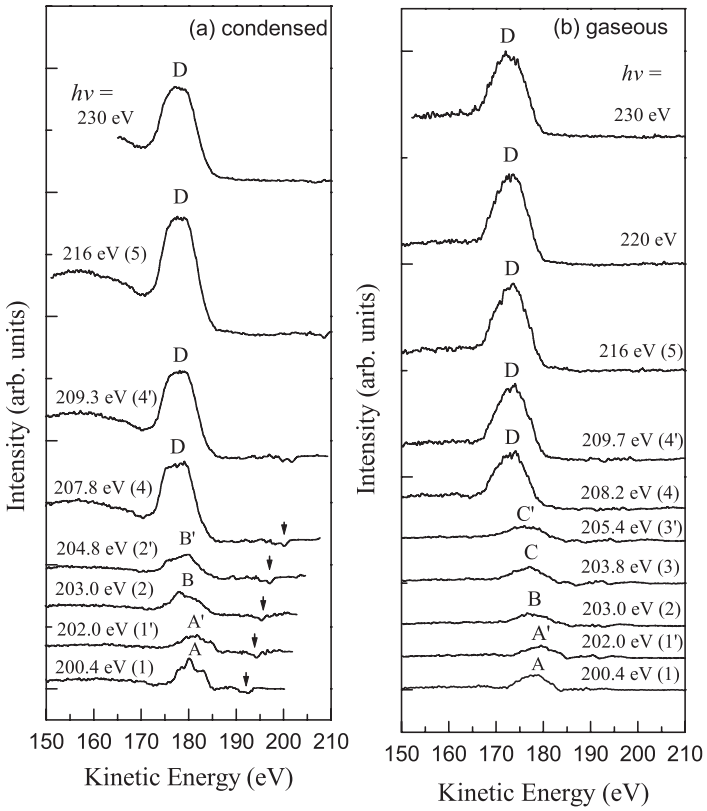

Figure 3. Auger spectra of (a) condensed CCl_4 (40 L exposure) and (b) gaseous CCl_4 for the difference between the photoemission spectra excited with various photon energies through the Cl L_{23}-edge absorption profile in figure 1 and the normal photoemission spectrum excited at 198 eV (shifted by the photon energy difference). The photon energy used for excitation is indicated in each spectrum. The number indicated in each spectrum corresponds to an absorption peak marked in the absorption spectrum in figure 1.

the intensity variations in the valence-band photoemission peaks are due to the contribution from participant Auger transitions and the change in cross section with photon energy.

In figures 3(a) and (b), Auger spectra of the difference between the photoemission spectra excited with various photon energies through the Cl L_{23}-edge absorption profile in figure 1 and the normal photoemission spectrum excited at 198 eV (shifted by the photon energy difference) of condensed and gaseous CCl_4 were reproduced, respectively. The kinetic energy presented in figure 3(a) is in reference to the Fermi level. The emission peaks labeled A, A′, B, B′, C and C′ in figures 3(a) and (b) are attributed to spectator Auger peaks. As noted from figure 3, following core-to-valence and core-to-Rydberg excitations, the intensity variations of the valence-band photoelectron peaks show a minor change, as indicated by arrows. This indicates that participant Auger decay makes a minor contribution to resonant Auger processes following excitations of Cl 2p to valence-states and Rydberg states. As noted, the total intensity of the spectator Auger peaks is an order of magnitude larger than that of the direct participant Auger process. Evidence of the predominance of the spectator Auger process can be seen from the pronounced intensity of the spectator Auger peaks labeled A, A, B, B′, C and C′, when the

photon energies vary through the Cl 2p core-to-valence and Cl 2p core-to-Rydberg resonances. This result reveals that the spectator Auger transitions prevail predominantly following the Cl 2p core-to-valence and Cl 2p core-to-Rydberg excitations that produce dominantly 2h1e states. In contrast, the shake-up excitation and shape-resonance excitation were followed by the normal Auger decay, because at even higher photon energies the normal Auger peak labeled D remains at the same kinetic energy.

As deduced from the resonant photoemission studies of condensed and gaseous CCl_4 in figure 3, the spectator Auger and normal Auger transitions were the dominant decay channels for the resonantly excited Cl 2p core holes, leading to the excited states with multiple holes in the valence orbitals. Accordingly, a close resemblance of the ion yield spectra and the Cl L-edge absorption spectra of condensed and gaseous CCl_4, as shown in figure 2, is attributed to the Auger decay of core-excited states and subsequent coulomb repulsion of the multi-valence-hole final states, which was called the Auger-initiated desorption (AID) mechanism [25, 26]. Besides this AID process, ion desorption from molecular adsorbates on surfaces can be induced by the secondary electrons produced by x-ray irradiation, so called x-ray induced electron-stimulated desorption (XESD) [27, 28]. It has been shown that, when the AID process is active, the contribution of the XESD process to ion desorption is minor for a thick layer [29, 30]. Thus, for the present thick CCl_4 coverage on Si(100) (>100 L exposure), the AID process would dominate over the desorption channel stimulated by secondary electrons. However, the state-specific enhanced production of Cl^+ yield in the condensed phase and CCl^+ in the gas phase via the Cl 2p $\rightarrow 7a_1^*$ excitation implies that an additional process exists for such an enhancement.

It was pointed out that the 2h1e state following the resonant core-level excitation is more effective for ion desorption than the 2 h state generated by the normal Auger transition [31]. If the spectator electron is localized in a strong antibonding orbital, the breaking of the chemical bond can be enhanced. In order to investigate atomic populations and molecular orbitals in CCl_4, the Gaussian 03 program was applied to perform all the calculations. The computations of the energies and molecular orbitals of CCl_4 were carried out in the ground state at the level of HF/6-31G* and MP2/6-311G*. Molecular orbitals and atomic populations were done for single-point calculations after geometry optimizations. Based on the molecular orbital calculations in CCl_4, the atomic populations of the C–Cl orbital, such as the $5a_1$ state, are mainly composed of the C 2s orbital and the Cl 3s orbital. It is therefore expected that the spectator electron in the C 3s* orbital or Cl 3s* orbital will assist in breaking the C–Cl bond. In addition, it is found that the $7a_1^*$ orbital is composed of C 2s (∼46%), Cl 3s (∼1.6%), Cl 3p (∼11%) and other minor components. The $8t_2^*$ orbital mainly consists of C 2s (<1%), Cl 3s (∼1.8%), C 2p (∼51%) and Cl 3p (∼10%). The content of the C 2s* orbital components in the $7a_1^*$ orbital is much higher than that in the $8t_2^*$ orbital. As a result, the spectator electron in the $7a_1^*$ orbital is more effective for the cleavage of the C–Cl bond than that in the $8t_2^*$ orbital.

Besides, the dissociated ion yields are found to be strongly correlated with the energy of the escaped ion that is related to the steepness of the potential surface of core-relaxed states [32, 33]. Thus, another possible reason for the significant difference in the Cl^+ yield following the excitations of Cl 2p to $7a_1^*$ and $8t_2^*$ states in figure 2(a) may be due to the difference in the steepness of the repulsive potential between $7a_1^*$ and $8t_2^*$. Perhaps the potential curve of $7a_1^*$ is steeper than that of $8t_2^*$. As a result, within the lifetime of 2h1e, Cl^+ can gain more kinetic energy from the $7a_1^*$ state, leading to lower ion reneutralization rates and consequently higher Cl^+ desorption yields [34]. In figure 4, the Cl^+ ion energy distributions of condensed CCl_4 following

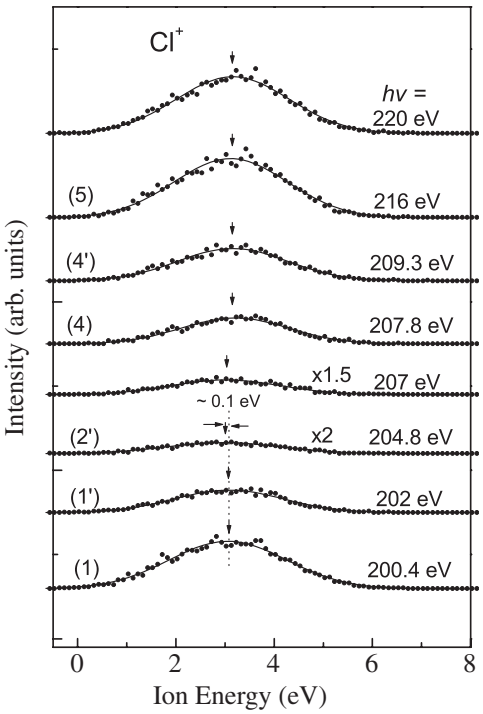

Figure 4. Cl^+ ion energy distributions for condensed CCl_4 following Cl 2p core-level excitations. The photon energy used for the excitation is indicated in each spectrum. The number indicated in each spectrum corresponds to an absorption peak marked in the TEY spectrum in figure 1(a). To ensure reproducible data, the ion kinetic energy distributions were recorded from 15 to 55 L exposure of CCl_4 on Si(100).

Cl 2p core-level excitations are reproduced. As noted, the Cl 2p $\rightarrow 7a_1^*$ excitation for condensed CCl_4 gives rise to an ion energy distribution higher ($\sim$0.1 eV) than the Cl 2p $\rightarrow 8t_2^*$ excitation, but lower ($\sim$0.1 eV) than the Cl 2p $\rightarrow$shape resonance excitation. Accordingly, the Cl 2p $\rightarrow 7a_1^*$ excitation leads to an enhancement of Cl^+ yield, as compared to the Cl 2p $\rightarrow 8t_2^*$ excitation. The enhancement of Cl^+ yield at the specific core-excited states is therefore strongly correlated with the energy of the escaped ion. This infers that the desorption of the Cl^+ ion is enhanced by a specific core-to-valence excitation with higher ion kinetic energy distribution.

In figure 5, the dispersed fluorescence spectrum of gaseous CCl_4 taken with an excitation photon of 230 eV is reproduced. The 237 nm peak is assigned to overlapping emission of excited $CCl^+(A^1\Pi - X^1\Sigma^+)$ and excited C atoms. The 254.9 nm peak is attributed to emission from excited C atoms [35]. The 278 nm peak is attributed to the excited $CCl(A^2\Delta - X^2\Pi)$ [35]. The emission peaks at 384, 480 and 521 nm have been ascribed to the excited Cl^+ ions [36]. Some emission features are due to a second-order light contribution from 254.9 and 384 nm, as indicated in figure 5. To elucidate how the various fluorescence pathways vary as a result of excitations of Cl 2p electrons to different empty orbitals, we monitored the relative yields of the excited fluorescing species observed in figure 5 as a function of photon energy in the vicinity of the Cl 2p edge. In figure 6, photon-energy dependence of the various excited fluorescing species observed in figure 5 in the vicinity of the Cl 2p edge is depicted along with the Cl

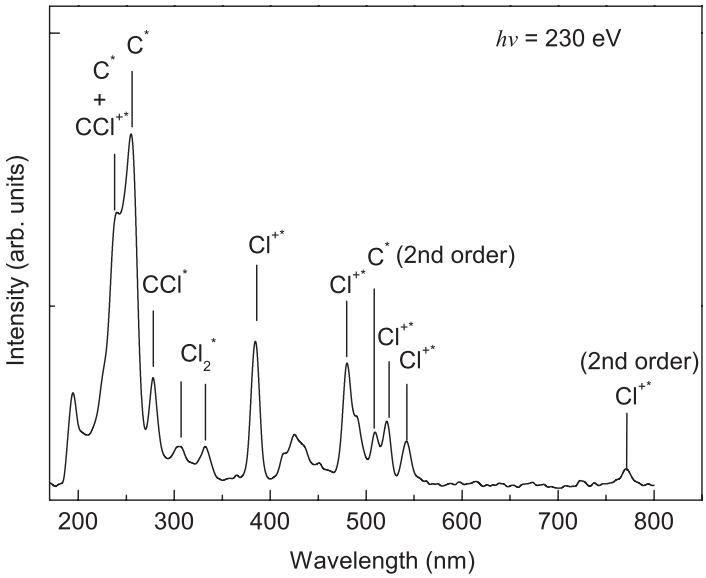

Figure 5. Dispersed fluorescence spectrum of gaseous CCl_4 following excitation with 230 eV photons.

L-edge x-ray absorption spectrum of gaseous CCl_4 for comparison. As noted from figure 6, the excitation spectra of excited Cl^+ resemble the Cl L_{23}-edge photoabsorption spectrum of gaseous CCl_4. In contrast, the relative intensities of valence-type peaks (labeled 1, 1′, 2 and 2′) and Rydberg-type peaks (labeled 3 and 3′) (indicated in figure 1) for fluorescence excitation spectra of excited neutral fragments (C^* and CCl^*) generated by CCl_4 molecules via the Cl 2p core-level excitation are notably different from that for Cl L-edge absorption spectrum of gaseous CCl_4. The excitations of Cl 2p core-electrons to Rydberg states (peaks 3 and 3′) and peaks 4 and 4′ lead to a noteworthy production of excited atomic neutral fragments (C^*) and excited diatomic neutral fragments (CCl^*). Similar to earlier studies on small core-excited molecules, a strong enhancement of the production of excited atomic and diatomic fragments is observed for resonant excitations of core-electrons to Rydberg states [9, 17, 37, 38]. Thus, this finding seems to be of a general nature. This infers that peaks 4 and 4′ in figure 1 have some Rydberg character. We therefore tentatively assigned discrete peaks 4 and 4′ in figure 1 as overlapping Rydberg-state and shake-up transitions [23].

As shown in figure 3, the spectator Auger transitions consist predominantly of gaseous CCl_4 following the Cl 2p core-to-valence and Cl 2p core-to-Rydberg excitations that produce dominantly 2h1e states. Based on the experimental results in figure 6, the 2h1e states with an excited Rydberg electron, as opposed to an excited valence electron, lead to enhanced production of the excited-state neutral fragments. One possible explanation for this enhancement is that the wavefunction of a diffuse Rydberg electron has less overlap with the molecular-ion core and consequently the 2h1e states dissociate to produce the excited-state fragments before the excited Rydberg electron can relax. As noted from figure 2(b), C^+ yield shows enhanced production via Cl 2p core-to-Rydberg excitations. This suggests that C^+ ions may be formed by a similar dissociation process to the one that produces the excited neutral fragments.

For dissociation mechanisms for ionic fragments, several mechanisms have been proposed [25]–[28]. However, the dissociation mechanism for neutral fragments, particularly

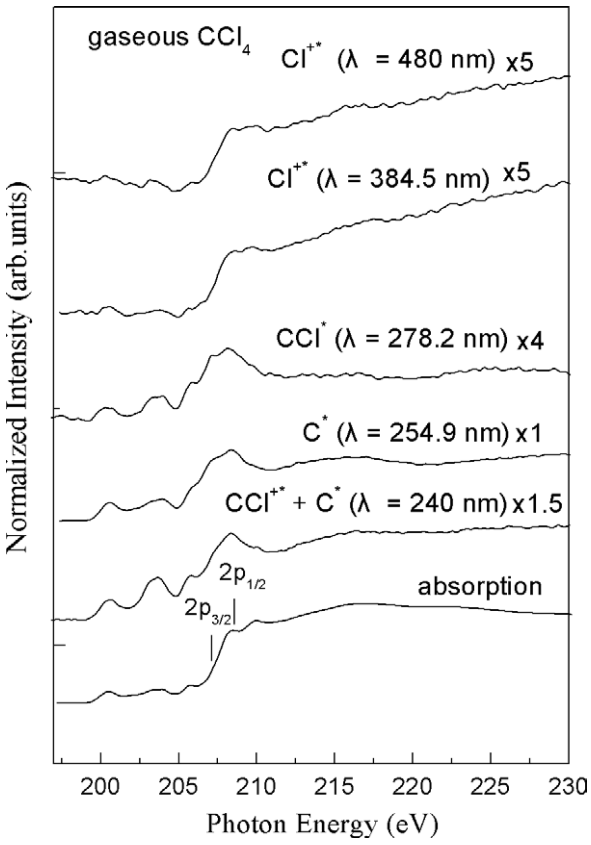

Figure 6. Photon-energy dependence of various excited fluorescing fragments at the Cl 2p edge along with the Cl L-edge x-ray absorption spectrum of gaseous CCl_4.

for gaseous molecules, is not clear at the moment [37]–[42]. To reveal the mechanism for excited neutral fragments and to explain the present data, detailed calculations of the potential-energy curves for highly excited molecular CCl_4^+ states are needed as well as further analysis of the Auger decay channels of CCl_4 at Rydberg resonances. Hopefully, our results will stimulate further theoretical development in the dissociation dynamics for excited neutral fragments of gaseous molecules.

4. Conclusion

In conclusion, we have investigated the dissociation dynamics for ionic fragments and excited neutral fragments of gaseous and condensed CCl_4 following the Cl 2p core-level excitation using photon-induced dissociation, resonant photoemission, ion kinetic energy distribution, x-ray absorption and UV/visible dispersed fluorescence measurements. The Cl $2p \rightarrow 7a_1^*$ excitation of CCl_4 induces significant enhancement of the Cl^+ desorption yield in the condensed phase and the CCl^+ yields in the gaseous phase. Based on the resonant photoemission studies, excitations of Cl 2p electrons to valence orbitals and Rydberg states decay predominantly via spectator Auger transitions, while the shake-up and shape-resonance excitations are followed by normal Auger decay. The Cl 2p core-to-Rydberg excitations of gaseous CCl_4 lead to a noteworthy

production of excited atomic neutral fragments (C^*) and excited diatomic neutral fragments (CCl^*). The present findings may be used to help assign the character of absorption features, by using the excitation spectrum of excited fragments as a fingerprint. These results contribute to a comprehensive understanding of the state-selective ionic and neutral fragmentation of gaseous and condensed molecules via core-level excitation.

Acknowledgments

We thank the NSRRC staff for their technical support. This research is supported by the NSRRC and the National Science Council of the Republic of China under grant nos NSC 95-2113-M-213-005, NSC 96-2113-M-213-009 and NSC 96-2113-M-213-007.

References

[1] Urisu T and Kyuragi H 1987 *J. Vac. Sci. Technol.* B **5** 1436
[2] Rosenberg R A, Frigo S P and Simons J K 1994 *Appl. Surf. Sci.* **79/80** 47
[3] Ueda K, Tanaka S, Shimizu Y, Muramatsu Y, Chiba H, Hayaishi T, Kitajima M and Tanaka T 2000 *Phys. Rev. Lett.* **85** 3129
[4] Baba Y, Yoshii K and Sasaki T A 1996 *J. Chem. Phys.* **105** 8858
[5] Nagaoka S, Mase K, Nagasono M, Tanaka S, Urisu T and Ohshita J 1997 *J. Chem. Phys.* **107** 10751
[6] Tinone M C K, Tanaka K, Maruyama J, Ueno N, Imamura M and Matsubayashi N 1994 *J. Chem. Phys.* **100** 5988
[7] Liu X J *et al* 2005 *Phys. Rev.* A **72** 042704
[8] Saito N, Bozek J D and Suzuki I H 1994 *Chem. Phys.* **188** 367
[9] Chen J M, Lu K T, Lee J M, Ma C I and Lee Y Y 2004 *Phys. Rev. Lett.* **92** 243002
[10] Nagaoka S I, Mase K and Kayano I 1997 *Trends Chem. Phys.* **6** 1
[11] Nenner I and Morin P 1996 *VUV and Soft X-Ray Photoionization* ed U Becker and D A Shirley (New York: Plenum)
[12] Simon M, Lebrun T, Martins R, De Souza G G B, Nenner I, Lavollee M and Morin P 1993 *J. Phys. Chem.* **97** 5228
[13] Baba Y 2003 *Low Temp. Phys.* **29** 228
[14] Svensson S 2005 *J. Phys. B: At. Mol. Opt. Phys.* **38** S821
[15] Ueda K 2003 *J. Phys. B: At. Mol. Opt. Phys.* **36** R1
[16] Ueda K and Eland J H D 2005 *J. Phys. B: At. Mol. Opt. Phys.* **38** S839
[17] Meyer M, Aloise S and Grum-Grzhimailo A N 2002 *Phys. Rev. Lett.* **88** 223001
[18] Romberg R, Heckmair N, Frigo S P, Ogurtsov A, Menzel D and Feulner P 2000 *Phys. Rev. Lett.* **84** 374
[19] Rosenberg R A, Wen C R, Tan K and Chen J M 1990 *Phys. Scr.* **41** 475
[20] Molin M J and Rowland F S 1974 *Rev. Geophys. Space Phys.* **13** 1
[21] Dixon-Warren S J, Heyd D V, Jensen E T and Polanyi J C 1993 *J. Chem. Phys.* **98** 5954
[22] Chen J M, Klauser R, Yang S C and Wen C R 1995 *Chem. Phys. Lett.* **246** 285
[23] Hitchcock A P and Brion C E 1978 *J. Electron Spectrosc. Relat. Phenom.* **14** 417
[24] Eberhardt W 1995 *Applications of Synchrotron Radiation: High-Resolution Studies of Molecules and Molecular Adsorbates on Surfaces* ed W Eberhard (Berlin: Springer) p 203
[25] Knotek L and Feibelman P J 1978 *Phys. Rev. Lett.* **40** 964
[26] Feibelman P J 1981 *Surf. Sci.* **102** L51
[27] Jaeger R, Stöhr J and Kendellewicz T 1983 *Surf. Sci.* **134** 547
[28] Jaeger R, Stöhr J and Kendellewicz T 1983 *Phys. Rev.* B **28** 1145
[29] Baba Y, Yoshii K and Sasaki T A 1997 *Surf. Sci.* **376** 330

[30] Chen J M, Yang S C and Liu Y C 1997 *Surf. Sci.* **391** 278
[31] Ramaker D E 1983 *Chem. Phys.* **80** 183
[32] Weimar R, Romberg R, Frigo S F, Kassühlke B and Feulner P 2000 *Surf. Sci.* **451** 124
[33] Chen J M, Lu K T, Lee J M, Chen C K and Haw S C 2006 *J. Chem. Phys.* **125** 214303
[34] Chen J M, Lu K T, Lee J M, Haw S C and Chang H W 2006 *Surf. Sci.* **600** 3544
[35] Kokue I, Honda T and Ito Y 1990 *Chem. Phys.* **140** 157
[36] Ralchenko Y, Jou F C, Kelleher D E, Kramida A E, Musgrove A, Reader J, Wiese W L and Olsen K 2006 *National Institute of Standards and Technology (NIST), Atomic Spectra Database Version 3.1.0*
[37] Meyer M, Marquette A and Gisselbrecht A 1999 *J. Electron Spectrosc. Relat. Phenom.* **101–103** 81
[38] Marquette A, Gisselbrecht M, Benten W and Meyer M 2000 *Phys. Rev.* A **62** 022513
[39] Romberg R, Frigo S P, Ogurtsov A, Feulner P and Menzel D 2000 *Surf. Sci.* **451** 116
[40] Wada S I, Matsumoto Y, Kohno M, Sekitani T and Tanaka K 2004 *J. Electron Spectrosc. Relat. Phenom.* **137–140** 211
[41] Feulner P, Romberg R, Frigo S P, Weimar R, Gsell M, Ogurtsov A and Menzel D 2000 *Surf. Sci.* **451** 41
[42] Melero García E, Kivimäki A, Pettersson L G M, Álvarez Ruiz J, Coreno M, de Simone M, Richter R and Prince K C 2006 *Phys. Rev. Lett.* **96** 063003